INSTITUTE OF PHYSICS PUBLISHING CLASSICAL AND QUANTUM GRAVITY

Class. Quantum Grav. **20** (2003) 2883–2903 PII: S0264-9381(03)58934-1

Numerical studies of Φ^2-oscillatons

Miguel Alcubierre[1], Ricardo Becerril[2], F Siddhartha Guzmán[3], Tonatiuh Matos[4], Darío Núñez[1] and L Arturo Ureña-López[5,6]

[1] Instituto de Ciencias Nucleares, Universidad Nacional Autónoma de México, AP 70-543, 04510 México, DF, Mexico
[2] Instituto de Física y Matemáticas, Universidad Michoacana, Edif. C-3, Ciudad Universitaria 58040, Morelia, Michoacán, Mexico
[3] Max-Planck-Institut für Gravitationsphysik, Am Mühlenberg 1, D-14476 Golm, Germany
[4] Departamento de Física, Centro de Investigación y de Estudios Avanzados del IPN, AP 14-740, 07000 México, DF, Mexico
[5] Astronomy Centre, University of Sussex, Brighton BN1 9QJ, UK

Received 28 January 2003
Published 12 June 2003
Online at stacks.iop.org/CQG/20/2883

Abstract

We present an exhaustive analysis of the numerical evolution of the Einstein–Klein–Gordon equations for the case of a real scalar field endowed with a quadratic self-interaction potential. The self-gravitating equilibrium configurations are called *oscillatons* and are closely related to boson stars, their complex counterparts. Unlike boson stars, for which the oscillations of the two components of the complex scalar field are such that the spacetime geometry remains static, oscillatons give rise to a geometry that is time dependent and oscillatory in nature. However, they can still be classified into stable (S-branch) and unstable (U-branch) cases. We have found that S-oscillatons are indeed stable configurations under small perturbations and typically migrate to other S-profiles when perturbed strongly. On the other hand, U-oscillatons are intrinsically unstable: they migrate to the S-branch if their mass is decreased and collapse to black holes if their mass is increased even by a small amount. The S-oscillatons can also be made to collapse to black holes if enough mass is added to them, but such collapse can be efficiently prevented by the gravitational cooling mechanism in the case of diluted oscillatons.

PACS numbers: 04.25.Dm, 95.30.Sf, 95.35.+d, 98.62.Ai, 98.80.−k

1. Introduction

In a seminal paper Seidel and Suen [1] found that there exist non-singular, time-dependent equilibrium configurations of self-gravitating real scalar fields. These oscillating soliton stars

[6] Present address: Instituto de Física de la Universidad de Guanajuato, A.P. E-143, C.P. 37150 León, Guanajuato, Mexico.

are called *oscillatons*, and are solutions of the Einstein–Klein–Gordon (EKG) system of equations for minimally coupled real scalar fields. The time dependence of these solutions appears as a fundamental ingredient that allows singularities to be avoided, in contrast to static solutions of the EKG equations with real scalar fields, where singularities frequently appear. The case of real scalar fields is quite different to that of complex scalar fields, for which the EKG equations provide the so-called boson stars, which are non-singular solitonic solutions with a static geometry (the components of the complex field oscillate in precisely such a way that the stress–energy tensor is time independent). However, the stability of oscillatons has not been studied in as much detail as in the case of boson stars [2–4]. Such studies are necessary because of the possible role of oscillatons in astrophysics and cosmology, where real scalar fields have been proposed as candidates for the dark matter in the Universe [5–7].

In this paper we want to complement previous studies [1, 3, 8–10] on oscillatons with a numerical analysis of the evolution of the EKG equations, much in the same way as has been done for boson stars [2–4]. The main aim is to investigate whether oscillatons are stable. For simplicity, we only consider here the spherically symmetric case of a real scalar field Φ endowed with a quadratic scalar potential of the form $V(\Phi) = (m^2/2)\Phi^2$. Other cases will be treated in future publications.

This paper is organized as follows. In section 2, we present the necessary mathematical background to find equilibrium configurations and to further evolve the EKG equations. As we shall see, the equilibrium configurations may be classified into two different groups: the S- and U-branches. The numerical methods and tests are presented in section 3. In sections 4 and 5, we analyse the results obtained from the evolution of the EKG equations for different oscillatons. We separately study the behaviour of S- and U-oscillatons by adding to them small and strong perturbations that change their total mass. We conclude in section 6.

2. Mathematical background

To begin with, we consider the spherically symmetric line element

$$ds^2 = -\alpha^2\,dt^2 + a^2\,dr^2 + r^2(d\theta^2 + \sin^2(\theta)\,d\varphi^2) \tag{1}$$

with $\alpha(r, t)$ being the lapse function and $a(r, t)$ being the radial metric function. We choose the polar-areal slicing condition (i.e. we force the line element to have the above form at all times, so that the area of a sphere with $r = R$ is always equal to $4\pi R^2$); this choice of gauge will force the lapse function $\alpha(r, t)$ to satisfy an ordinary differential equation in r. Throughout the work, we will be using units such that $c = \hbar = 1$, and we express the gravitational constant in terms of the Planck mass: $G = 1/m_{\rm Pl}^2$.

The energy–momentum tensor of a scalar field Φ endowed with a quadratic self-interaction potential $V(\Phi) = (m^2/2)\Phi^2$ is

$$T_{\mu\nu} = \Phi_{,\mu}\Phi_{,\nu} - \frac{g_{\mu\nu}}{2}[\Phi^{,\sigma}\Phi_{,\sigma} + m^2\Phi^2]. \tag{2}$$

The non-vanishing components of $T_{\mu\nu}$ are

$$-T^0{}_0 = \rho_\Phi = \tfrac{1}{2}[\alpha^{-2}\dot{\Phi}^2 + a^{-2}\Phi'^2 + m^2\Phi^2], \tag{3}$$

$$T_{01} = \mathcal{P}_\Phi = \dot{\Phi}\Phi', \tag{4}$$

$$T^1{}_1 = p_r = \tfrac{1}{2}[\alpha^{-2}\dot{\Phi}^2 + a^{-2}\Phi'^2 - m^2\Phi^2], \tag{5}$$

$$T^2{}_2 = p_\perp = \tfrac{1}{2}[\alpha^{-2}\dot{\Phi}^2 - a^{-2}\Phi'^2 - m^2\Phi^2], \tag{6}$$

and also $T^3{}_3 = T^2{}_2$. These different components are identified as the energy density ρ_Φ, the

momentum density $\mathcal{P}_\Phi$, the radial pressure p_r and the angular pressure $p_\perp$. The parameter m is interpreted as the mass of the scalar particles. Overdots denote $\partial/\partial t$ and primes denote $\partial/\partial r$.

The evolution of the metric functions α and a can be obtained from the Einstein equations $G_{\mu\nu} = \kappa_0 T_{\mu\nu}$, with $\kappa_0 = 8\pi G$. In order to write appropriate evolution equations, we now introduce the first order variables $\Psi = \Phi_{,r}$ and $\Pi = a\Phi_{,t}/\alpha$. Also, we define the dimensionless quantities $r = x/m, t \to t/m, \Phi \to \Phi/\sqrt{\kappa_0}$, where we note that the bosonic mass is the natural scale for time and distance.

Using these new variables, the Hamiltonian constraint becomes

$$\frac{a_{,x}}{a} = \frac{1-a^2}{2x} + \frac{x}{4}[\Psi^2 + \Pi^2 + a^2\Phi^2] \tag{7}$$

and the polar-areal slicing condition takes the form

$$\frac{\alpha_{,x}}{\alpha} = \frac{a_{,x}}{a} + \frac{a^2-1}{x} - xa^2\Phi^2. \tag{8}$$

The evolution of the scalar field Φ is governed by the Klein–Gordon (KG) equation, which appears as a consequence of the conservation equations of the scalar field energy–momentum tensor (2) in the form

$$T^{\mu\nu}{}_{;\nu} = \Phi^{,\mu}(\Box - m^2)\Phi = 0, \tag{9}$$

where $\Box = g^{\alpha\beta}\nabla_\alpha\nabla_\beta$ is the d'Alembertian operator. The KG equation is equivalent to the following set of first order differential equations

$$\Phi_{,t} = \frac{\alpha}{a}\Pi, \tag{10}$$

$$\Pi_{,t} = \frac{1}{x^2}\left(\frac{x^2\alpha\Psi}{a}\right)_{,x} - a\alpha\Phi, \tag{11}$$

$$\Psi_{,t} = \left(\frac{\alpha\Pi}{a}\right)_{,x}. \tag{12}$$

Equations (7)–(12) form the complete set of differential equations to be solved numerically.

2.1. Eigenvalue problem for equilibrium configurations

In order to find the equilibrium configurations of oscillatons, equations (7)–(12) are solved using Fourier expansions for both the metric and the scalar field functions [1, 8–10]. We briefly describe here the procedure used in [9] to find such equilibrium configurations.

In order to deal with the non-linearities present in the EKG equations, it is convenient to introduce the new variables $A(t,r) = a^2(t,r), C(t,r) = (a/\alpha)^2$, for which equations (7)–(12) take the form

$$A_{,x} = \frac{Ax}{2}\left(C\Phi_{,t}^2 + \Phi_{,x}^2 + A\Phi^2\right) + \frac{A}{x}(1-A), \tag{13}$$

$$C_{,x} = \frac{2C}{x}\left[1 + A\left(\frac{1}{2}x^2\Phi^2 - 1\right)\right], \tag{14}$$

$$C\Phi_{,t,t} = -\frac{1}{2}C_{,t}\Phi_{,t} + \Phi_{,x,x} + \Phi_{,x}\left(\frac{2}{x} - \frac{C_{,x}}{2C}\right) - A\Phi, \tag{15}$$

$$A_{,t} = xA\Phi_{,t}\Phi_{,x}. \tag{16}$$

The lapse function is later obtained as $\alpha^2(t,x) = A(t,x)/C(t,x)$. Note that equation (16) is a consequence of the momentum constraint (the $\{t,r\}$ part of the Einstein equations).

We shall consider the Fourier expansions

$$\Phi(t,x) = \sum_{j=1}^{j_{\max}} \phi_j(x)\cos(j\omega t), \qquad A(t,x) = \sum_{j=0}^{j_{\max}} A_j(x)\cos(j\omega t),$$
$$C(t,x) = \sum_{j=0}^{j_{\max}} C_j(x)\cos(j\omega t), \tag{17}$$

where ω is called the fundamental frequency and $j_{\max}$ is the mode at which the Fourier series are truncated.

Solutions are obtained by introducing the Fourier expansions (17) in equations (13)–(16), and setting each Fourier coefficient to zero. After introducing $\xi(x) = \phi_{,x}(x)$, the EKG equations are reduced to a set of coupled first order ordinary differential equations of the form

$$\frac{\mathrm{d}X_j}{\mathrm{d}x} = {}_X F_j(X_k), \tag{18}$$

where X_j could be $A_j(x), C_j(x), \phi_j(x)$ or $\xi_j(x)$. In ${}_X F_j$ there are non-linear terms, for instance $A(x,t)C(x,t)$, which should be written as a Fourier expansion with coefficients $(AC)_k(x)$. These coefficients can be obtained using convolution sums.

The boundary conditions are determined by requiring non-singular and asymptotically flat solutions, for which equations (13)–(16) become an eigenvalue problem. Thus, it is only necessary to determine the initial values $\phi_i(0), C_i(0)$ (the fundamental frequency is an *output* value) corresponding to a given central value $\phi_1(0)$, to obtain different equilibrium configurations. To find these values, we employed the shooting method. In practice, only the odd coefficients in the scalar field expansion and the even coefficients in the metric functions A and C are required. For the coefficients A_j, we only integrated $\frac{\mathrm{d}A_0}{\mathrm{d}x} = {}_A F_0$ and find the remaining $A_{j\leqslant 1}$ by using the algebraic relation (16). Given $j_{\max}$ there are $2 + 3j_{\max}$ ordinary differential equations. We solved them with an adaptive stepsize control Runge–Kutta method.

A typical oscillaton solution is shown in figure 1. Even though we are solving non-linear equations, the Fourier series converges rapidly. A particular feature of the solutions is that they are represented only by odd Fourier coefficients of the scalar field Φ and the even coefficients of the metric functions A and C.

In figure 2, we show the calculated total mass (M_{T}), the fundamental frequency ($\Omega \equiv \omega/m$) and the radius at which the radial metric coefficient reaches its maximum value at $t = 0$ ($R_{\max}(0)$) for different configurations. In the case of oscillatons, the position of the maximum of a^2 is not a fixed value but instead oscillates in time. However, as we shall see below (see figure 9), the amplitude of such oscillations is quite small and the initial value can be taken as representative of each oscillaton. The maximum mass $M_c = 0.607 m_{\mathrm{Pl}}^2/m_\Phi$ is reached for a central value $\phi_{1c}(0) = 0.48$, to which also corresponds a fundamental frequency $\Omega = 0.864$. The fundamental frequency is always such that $\Omega \leqslant 1$ for all oscillatons, with $\Omega = 1$ for the trivial solution. In general, more massive oscillatons oscillate with a smaller fundamental frequency.

3. Numerics

3.1. Numerical algorithm for the evolution of the system

In order to integrate the Klein–Gordon equations (10)–(12), we used a method of lines with second order centred differences in space. For the time integration we use a method

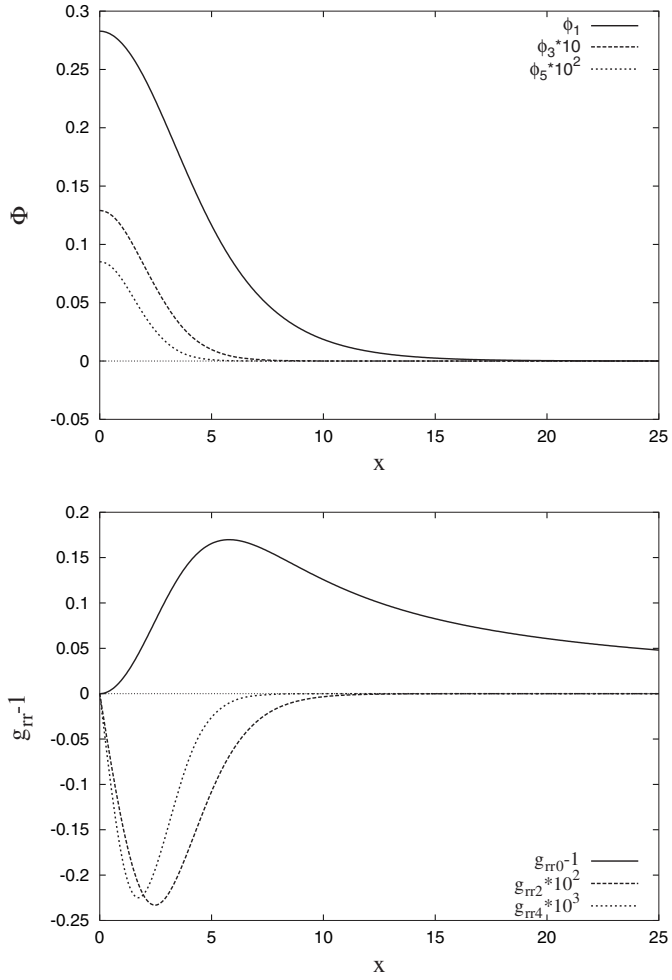

Figure 1. Non-zero Fourier coefficients of the scalar field Φ and the radial metric coefficient $g_{rr}-1$ (see equations (17)) for a configuration with $\phi_1(0) = 0.2828$. The total mass is $M = 0.5726 m_{\rm Pl}^2/m$ and the fundamental frequency is $(\omega/m) = 0.9128$. The solution shown here was calculated up to the sixth Fourier mode ($j_{\max} = 6$ in equations (17)). The convergence of the Fourier series is manifest (notice the re-scaling of the higher Fourier modes).

inspired in the iterative Crank–Nicholson (ICN) scheme with three iterations (see for example [12, 13]). The standard ICN is used to integrate a system of evolution equations of the form:

$$\frac{\partial u_i}{\partial t} = S_i(u_j, \partial_{x_k} u_j). \tag{19}$$

Given values of the variables u_i at time step $t = n\Delta t$, one updates the values of the variables to time step $t = (n+1)\Delta t$ in the following way:

$$u_i^{(1)} = u_i^n + (\Delta t/2) S_i^n, \tag{20}$$

$$u_i^{(k)} = u_i^n + (\Delta t/2) S_i^{(k-1)}, \qquad k = 2, \ldots, N-1, \tag{21}$$

$$u_i^{n+1} = u_i^n + \Delta t S_i^{(N-1)}, \tag{22}$$

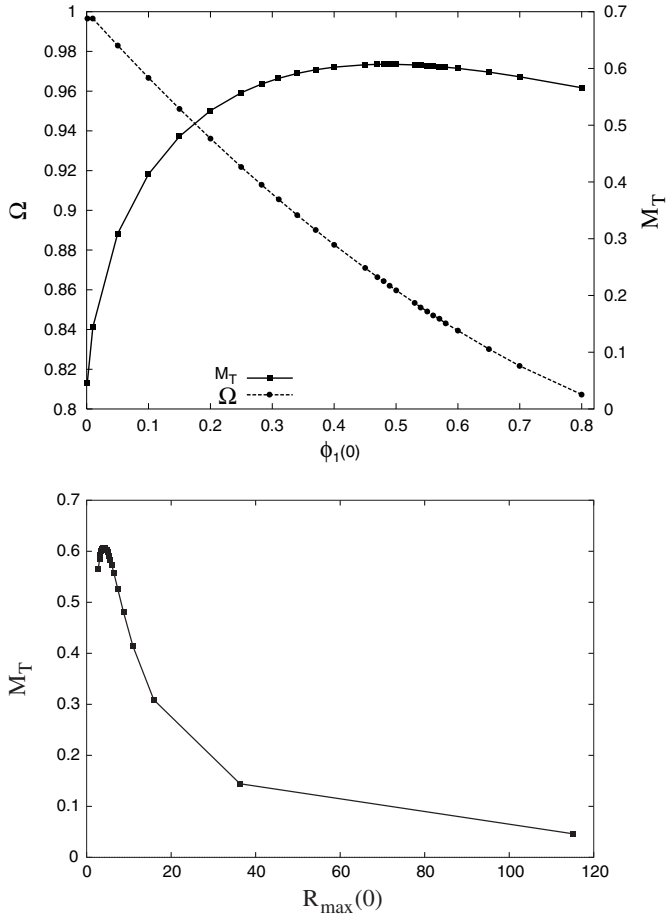

Figure 2. (Top) Total masses $M_{\rm T}$ (in units of $m_{\rm Pl}^2/m_\Phi$) and fundamental frequencies (Ω) of different oscillatons. The critical (maximum) mass is $M_{\rm c} = 0.607 m_{\rm Pl}^2/m_\Phi$ for a configuration with a central value $\phi_{1_{\rm c}}(0) = 0.48$; its corresponding frequency is $(\omega/m) = 0.864$. (Bottom) Plot of the total mass $M_{\rm T}$ versus $R_{\rm max}(0)$ (the latter in units of m^{-1}), the radius at which the metric coefficient g_{rr} reaches its maximum value at $t = 0$.

where $u_i^n = u_i(t = n\Delta t)$, $u_i^{n+1} = u_i(t = (n+1)\Delta t)$ and $u_i^{(k)}$ are intermediate values. Taking $N = 3$ is enough to obtain a second order accurate, stable scheme [12, 13] (in fact, taking $N = 2$ is enough for second order accuracy, but it is unstable).

For our purposes we have modified the above algorithm for the case $N = 3$ in the following way:

$$u_i^{(1)} = u_i^n + (\Delta t/3) S_i^n, \tag{23}$$

$$u_i^{(2)} = u_i^n + (\Delta t/2) S_i^{(1)}, \tag{24}$$

$$u_i^{n+1} = u_i^n + \Delta t\, S_i^{(2)}. \tag{25}$$

The reason for this modification is that the above scheme is considerably less dissipative than standard three-step ICN. In fact, for linear equations one can show that the above scheme is third order in time. We have found our modified scheme ICN to be very stable and robust in practice.

Once we have advanced the variables Φ, Ψ and Π one time step using the above algorithm, we substitute their new values into equations (7) and (8). These are simple ordinary differential equations on the radial coordinate that we solve using a standard second order Runge–Kutta scheme.

3.2. Boundary conditions

Our set of equations is singular at $x = 0$. To avoid the singularity, we stagger the origin and take a spatial grid of the form $x_i = (i - 1/2)\Delta x$. The fictitious point at $x_0 = -\Delta x/2$ is used to impose appropriate parity conditions: Π is even and Ψ is odd. Note that we can integrate Φ all the way to the boundary point $x_0 = -\Delta x/2$, since its evolution equation does not require the evaluation of spatial derivatives.

At the outer boundary we also need to impose boundary conditions. Note again that we do not need to apply a boundary condition for Φ, as its evolution equation can be integrated all the way to the boundary point. For Π we assume that, for large enough x, it behaves as an outgoing wave pulse of the form:

$$\Pi = u(x - t)/x, \tag{26}$$

with u being an arbitrary function. In differential form this becomes

$$\partial_x \Pi + \partial_t \Pi + \Pi/x = 0, \tag{27}$$

which, by performing finite difference, can be solved for the unknown boundary value at the new time level. On the other hand, it is not difficult to convince oneself that the function Ψ does not behave as an outgoing wave at the boundary. However, we are assuming that Π does and, as a consequence, so does Φ. In particular, the outgoing wave boundary condition applied to Φ can be seen to imply that at the boundary:

$$\Psi = -\Pi - \Phi/x. \tag{28}$$

This equation can then be used to obtain boundary values for Ψ once those of Φ and Π are known.

Finally, we need to mention the boundary conditions used for the ordinary differential equations that have to be solved to find the metric functions α and a. For a, we use the fact that local flatness implies that $a(x = 0) = 1$ and $\partial_x a(x = 0) = 0$. These two conditions imply that $a(x_0) = a(x_1) = 1 + \mathcal{O}(\Delta x)^3$. We use these two boundary values at the first two grid points and integrate the second order Hamiltonian constraint outwards.

For the lapse function α we use the fact that, in a vacuum, our slicing condition implies that we are in Schwarzschild coordinates, so we must have $\alpha = 1/a$. We then assume that our boundaries are sufficiently far away as to be always in a vacuum, and impose $\alpha = 1/a$ as an outer boundary condition. The slicing condition is then integrated inward. One could presumably improve on this by setting $\alpha(x = 0) =$ constant, $\partial_x \alpha(x = 0) = 0$ as boundary conditions on the origin, integrating the slicing condition outwards, and then re-scaling it so that the lapse goes as $1 + k/x$ far away (k is a constant, note that the slicing condition is scale invariant).

3.3. Regularity at the origin

Among the evolution equations for the scalar field (10)–(12), the one corresponding to Π could be particularly problematic when discretized without care, because it is not second order accurate due to the presence of the factor $1/x^2$ in the principal part. Nevertheless, a simple

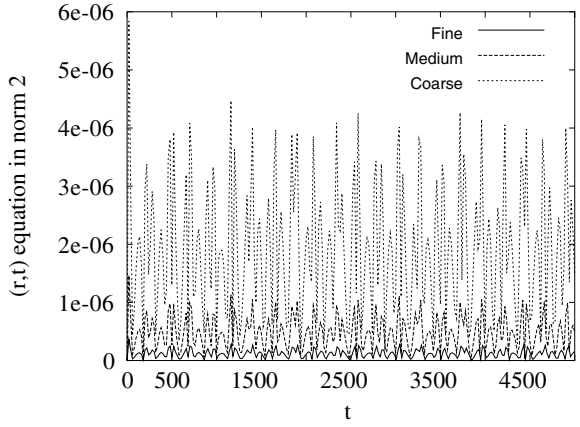

Figure 3. The momentum constraint (30) for three different resolutions: fine (d$r = 0.01$), medium (d$r = 0.02$) and coarse (d$r = 0.04$). The initial conditions correspond to a Gaussian pulse of the form $\Phi(0, x) = 0.296\,\mathrm{e}^{-x^2/5.35}$, and total mass $M = 0.575$. The numerical code remains second order convergent.

transformation of (11) that warranties the accuracy of our simulations at the origin reads as follows

$$\Pi_{,t} = 3\frac{\partial}{\partial x^3}\left(\frac{x^2\alpha\Psi}{a}\right) - a\alpha\Phi, \tag{29}$$

which is the equation we discretized. Note that the first term on the right-hand side of this equation includes now a first derivative with respect to x^3 and not a third derivative (see [11]).

3.4. Code tests

3.4.1. Accuracy. In order to illustrate how all these ingredients work together properly, we now study the accuracy of our numerical methods in some particular cases. In figure 3 we show the convergence of a system initially consisting of a Gaussian pulse of scalar field. The equation we use to calibrate our techniques is the (r, t) component of Einstein's equations (the momentum constraint):

$$\beta := a_{,t} - \tfrac{1}{2}x\alpha\Phi\Pi = 0, \tag{30}$$

which should be satisfied for an exact solution[7]. What we show in the plot is the $L2$ norm of the value of β across the grid as a function of time for three different resolutions. The initial Gaussian corresponds to an oscillaton with $M = 0.575$, so that it is in the stable branch and has a long time life; the boundary is located at $x = 50$ so that the evolutions were carried out up to 100 crossing times. The fact that the value of β goes down by a factor of 4 every time the resolution is doubled shows that the code remains second order convergent.

3.4.2. Effects of the boundary. Since we are using boundary conditions corresponding to the Klein–Gordon equation without a mass term, it means that part of the scalar field has to be reflected from the boundaries. In order to estimate the inaccuracy of our method, we choose the same system as above with the coarse resolution. In figure 4 we show the function $x^2\rho$ at

[7] In a previous work [1], the component momentum constraint was used to evolve a and the Hamiltonian constraint was monitored to calibrate the accuracy of the numerical methods. In this paper we have decided to do the opposite.

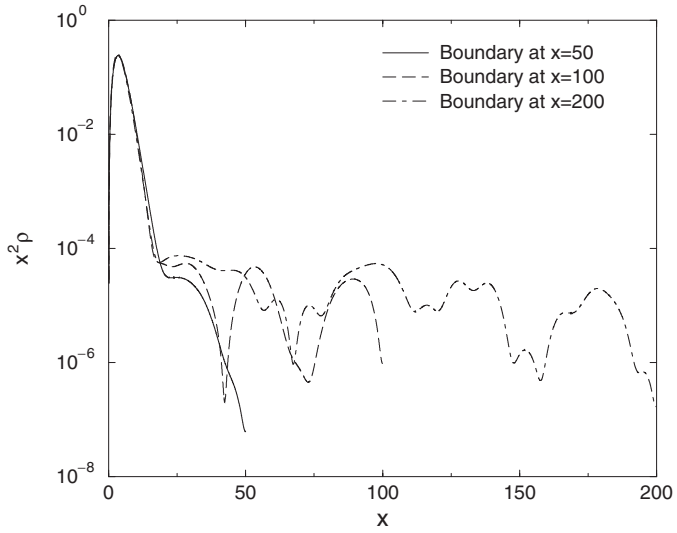

Figure 4. The function $x^2\rho$ is shown for different locations of the boundaries at $t = 4000$ for the system above. It is evident that after many crossing times the non-exact boundary conditions used start introducing reflections.

$t = 4000$ for three different situations: the system is evolved with boundaries at $x = 50$, 100 and 200. It is clear that the different evolutions coincide very well up to $x = 20$ but differ significantly outside, where $x^2\rho < 10^{-4}$ in the present case. This certainly indicates that at such regions the effects of the boundary dominate our simulations over such large periods of time (see also [6]).

4. Evolution of oscillatons: the S-branch and the quasi-normal modes

We shall call S-branch oscillatons those equilibrium configurations to the *left*-hand side of the critical configuration in the plot M versus $\phi_1(0)$ in figure 2 (or equivalently, those configurations to the *right*-hand side in the plot of M versus $R_{\max}$). As a first step in the study of the stability of oscillatons, we will numerically evolve these equilibrium configurations.

We should keep in mind that, compared to oscillatons constructed with the full series expansion, the solutions presented in figure 2 are already perturbed. These perturbations arise because of the inherent discretization error of the numerical solutions and (mainly) the truncated Fourier expansions. Therefore, the eigensolutions in section 2.1 will be treated as already *slightly perturbed* profiles [1].

The main results presented in this section can be summarized as follows. (i) S-oscillatons are stable against *small* perturbations. (ii) Besides the fundamental oscillations of the system, there is an overall vibration of the oscillaton when slightly perturbed. The frequencies (f) of these vibrations could be identified with the so-called quasi-normal modes of the system, since the geometry of the perturbed configurations decays to one corresponding to an equilibrium configuration, though a formal analysis will be required in the future to investigate whether or not it is an exponential decay. The plot of f versus M found is a particular feature of the Φ^2-oscillatons as it has also been shown to be for boson stars. As we shall see below, such quasi-normal modes are very important in the study of the evolution of these systems.

We consider the scalar field profiles obtained by solving equations (15) and (16) to be the initial data for the evolution equations. In this form, the initial conditions for the scalar field are (see equations (17))

$$\Phi(t=0,x) = \sum_{j=1}^{j_{\max}} \phi_j(x) \tag{31}$$

$$\Phi'(t=0,x) = \sum_{j=1}^{j_{\max}} \phi'_j(x) \tag{32}$$

$$\dot{\Phi}(t=0,x) = 0 \tag{33}$$

and then the metric functions α, a are calculated through the Einstein equations. In this manner, we will also check the consistency between the eigenvalue problem and the numerical evolution since no additional information (such as the metric functions, the fundamental frequency ω, etc) is taken initially.

As a typical example of an S-branch oscillaton, we show in figure 5 the evolution of the initial profile shown in figure 1, characterized by the central value $\phi_1(0) = 0.2828$. From the figure we see that such an oscillaton is stable, maintaining the same oscillatory pattern from $t \simeq 300$ (see figure 6) up to times $t \simeq 20\,000$ (in the plot we are showing only a fraction of the run). That the evolution is stable can also be seen from figure 6, in which we show the accuracy of the numerical evolution by plotting the momentum constraint. In figure 7 we show the evolution of the total integrated mass. We can see a small appreciable adjustment of the original mass at around $t = 300$, indicating a small ejection of the scalar field from the system. The overall linear decay of the mass can be shown to be consistent (using convergence tests) with a small amount of numerical dissipation still present in our numerical method, and is therefore not an intrinsic decay of the oscillaton.

The simulations show that the evolved geometry of our initial data oscillates periodically at two different time scales. In particular, there is a short-period oscillation corresponding to the expansion (17), that is, the fundamental oscillation, and an overall vibration with a longer period [1]. We shall refer to the latter as the quasi-normal modes of the oscillatons.

To determine the oscillatory scales of the solution, we calculated the Fourier transform of the evolution of $(g_{rr})_{\max}$ in figure 5, and plotted it in figure 8. Note that the dominant frequencies are the quasi-normal one and the fundamental angular frequency, which are, respectively, $(f/m) = 4.52 \times 10^{-2}$ and $(\omega/m) = 0.9119$. Higher modes corresponding to even multiples of the fundamental frequency are also present, but their power is smaller.

We systematically evolve all other S-branch equilibrium configurations shown in figure 2, calculating their corresponding power spectrum and then their quasi-normal and fundamental frequencies. In all cases, the evolved profiles behaved accordingly with the description given above for the (representative) case $\phi_1(0) = 0.2828$. For instance, the values of the fundamental frequencies coming out from our Fourier analysis of the evolved systems were only slightly different from those proposed in the series (17), coinciding up to four digits. In general, the power spectrum of more dilute oscillatons is dominated by the fundamental frequency, while the quasi-normal frequency dominates for oscillatons near the critical point. Also, the linear numerical dissipation of mass was as in figure 6, suggesting also that it should be attributed to the numerical method and not to the intrinsic properties of oscillatons.

The resulting plot of f versus M in figure 8 has been very useful to analyse the evolution of boson stars [2, 4], and we will see it is useful for oscillatons as well. The plot shows a maximum and a sharp decline near the critical mass. This is a typical behaviour indicating the transition from stable to unstable configurations.

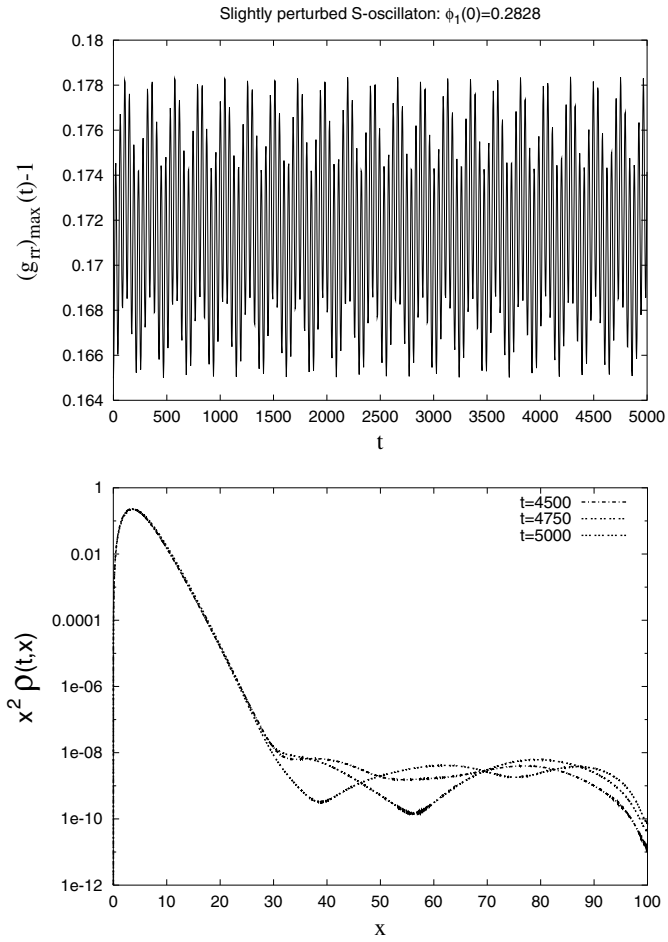

Figure 5. (Top) Maximum values of the radial metric function $g_{rr}(t, x) = a^2(t, x)$. The initial configuration is that of figure 1 with $\Delta x = 0.01$, $\Delta t/\Delta x = 0.5$. The boundary is at $x = 100$ and the evolution is shown to $t = 5000$ m^{-1}, some 50 crossing times. In fact, we have followed the run up to $t = 20\,000$ m^{-1} and no change was observed. Thus, we can conclude that the initial configuration is stable against *small* perturbations. (Bottom) The density profile $\rho_\Phi(t, x)$ times x^2 is plotted for late times.

To further demonstrate that the S-oscillatons are stable and that the frequencies shown in figure 8 are their intrinsic quasi-normal modes, we show in figure 9 the evolution of the total mass $M_{\rm T}$ and $R_{\rm max}$ compared to the equilibrium configurations as shown in figure 2. It is clear that the slightly perturbed S-oscillatons oscillate with very small amplitudes around the original equilibrium configurations. In other words, they are not migrating to other oscillatons nor decaying. This can be compared to the migrating oscillatons shown in figures 11, 13 and 14.

The results presented above give evidence for points (i) and (ii) outlined at the beginning of this section. We would like to stress here that the important result is that there do exist stable oscillatons (at least in the S-branch). As a side effect, we have also shown the consistency between the eigenvalue problem and the numerical evolution code.

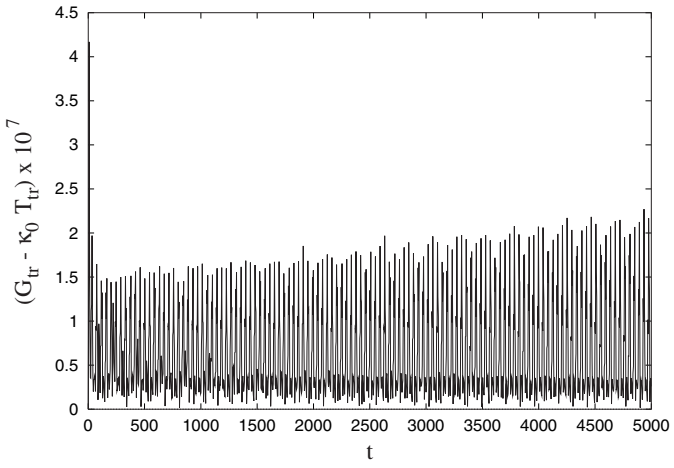

Figure 6. The $L2$ norm of the momentum constraint for the numerical evolution of the oscillaton shown in figures 1 and 5.

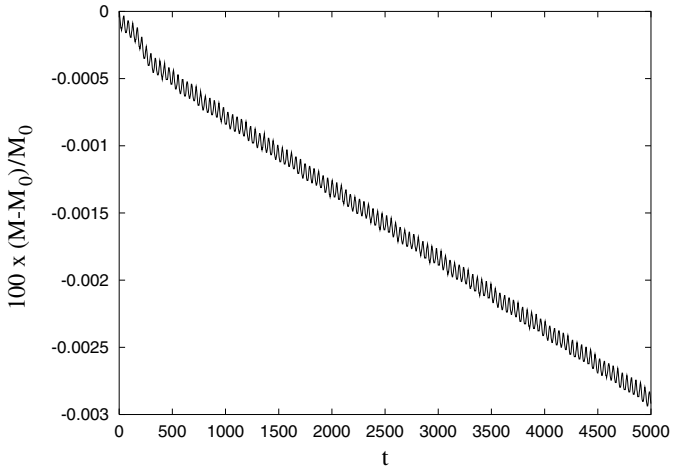

Figure 7. Total integrated mass as a function of time during the evolution of the same oscillaton. We see that the oscillaton ejects a very small amount of matter at around $t = 300\ \mathrm{m}^{-1}$. The overall linear decrease is due to the numerical dissipation still present in the code.

4.1. Perturbed S-oscillatons

Our interest now is to determine whether S-branch oscillatons are stable against *strong* perturbations. That is, we want to know the conditions under which such oscillatons will collapse into a black hole, disperse away or form another oscillaton. The last case is a rather interesting possibility since, as we shall show below, it implies the migration of oscillatons.

We have included Gaussian-like perturbations in the original equilibrium configurations, as shown in figure 10, which can be seen just as perturbations to the original mass of the oscillatons. (We shall call *original* the profiles shown in figure 2 and their corresponding parameters). The main results are summarized as follows. (iii) If an oscillaton is perturbed

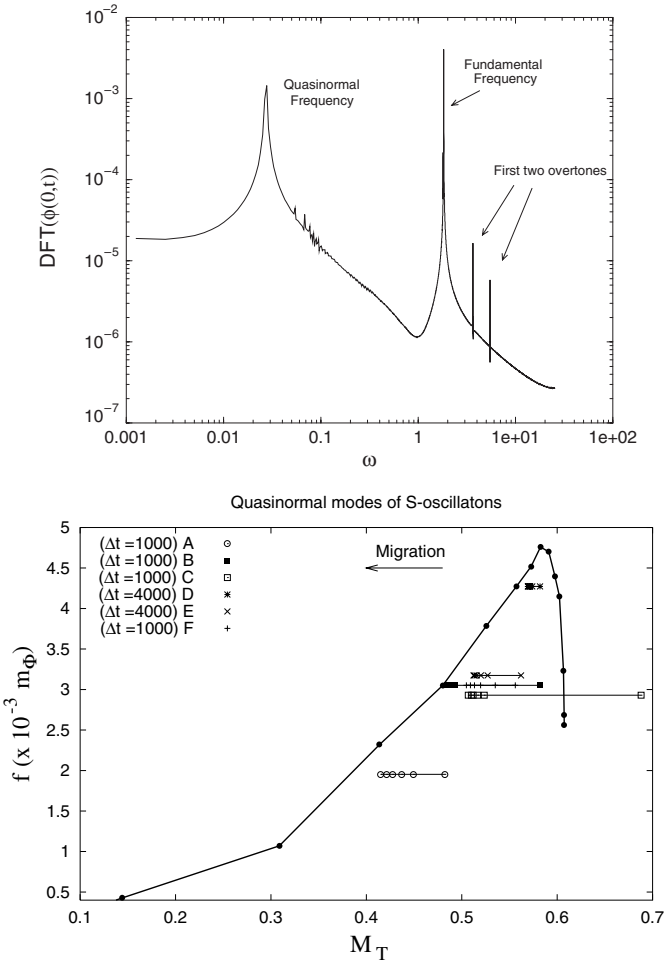

Figure 8. (Top) The Fourier transform of the evolution of the metric coefficient g_{rr} for the case in figure 5. The configuration vibrates with the quasi-normal frequency $(f/m) = 4.52 \times 10^{-2}$ while it oscillates with even multiples of the fundamental angular frequency $(\omega/m) = 0.9119$. The latter coincides with the result of the eigenvalue problem (see figure 1). (Bottom) The frequencies of the quasi-normal modes obtained from the evolution of slightly perturbed S-branch oscillatons. We also show the migration of perturbed S-branch and U-branch oscillatons, labelled A–F; the details of their evolution can be found in sections 4.1 and 5. In the plot, Δt represents the time intervals at which the evolved mass was measured for each case.

in such a way that its mass is less than the critical mass $M_c \simeq 0.606(m_{Pl}^2/m)$,[8] it migrates to another solution in the S-branch; and (iv) on the other hand, if the initial mass is larger than M_c, the oscillaton can either migrate to an S-oscillaton or collapse to a black hole. The collapse to a black hole can be prevented by the oscillaton ejecting the mass excess. This mechanism is highly effective for dilute oscillatons. In both cases (iii) and (iv) above, the evolution of the perturbed profiles can be tracked according to their vibration frequencies, i.e., the quasi-normal modes. We have plotted some typical evolutions of perturbed S-branch oscillatons in figure 11 which show the different behaviour described above.

[8] This value is just 0.16% lower than that determined from the eigenvalue problem in section 2.1 (see also section 5.2).

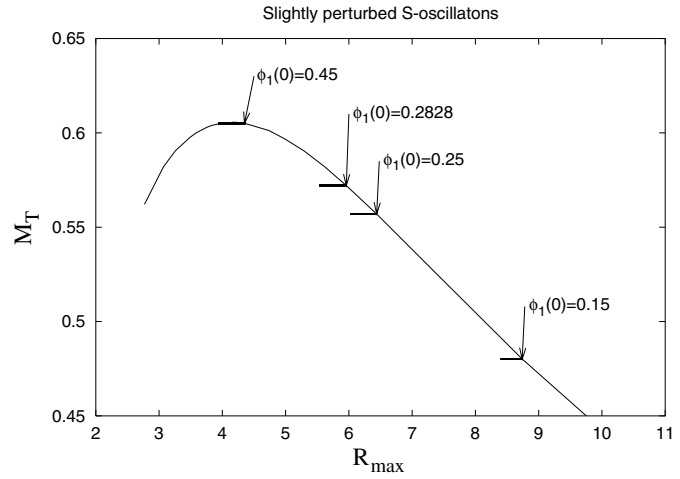

Figure 9. The evolution of the total mass $M_{\rm T}$ and $R_{\rm max}$ is shown for different S-oscillatons. The runs were followed up to $t = 5000\ {\rm m}^{-1}$. It can be clearly seen that the evolutions proceed just by small oscillations around the initial profiles. Actually, since the profile in figure 2 uses the initial value $R_{\rm max}(0)$, the oscillations are shifted to the *left* of the solid line. Hence, it is manifest that these oscillatons are not migrating nor decaying. For a comparison with truly migrating oscillatons, see figures 11, 13 and 14.

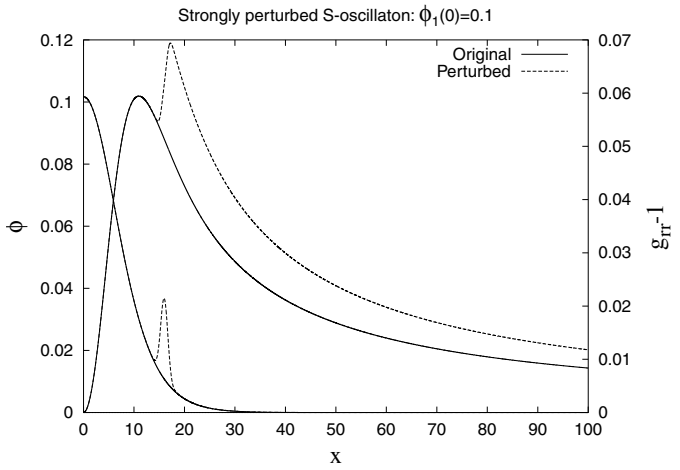

Figure 10. Examples of the scalar field and g_{rr} profiles of a strongly perturbed S-oscillaton by means of a Gaussian perturbation. Shown is the case of a $\phi_1(0) = 0.1$ oscillaton whose original mass was increased by 40%. The evolution of this oscillaton is given in figures 8 (label B), 12 and 11 (see also text below for details).

We start by discussing point (iii). In the first case, we decreased the initial mass of a $\phi_1(0) = 0.45$ oscillaton to an initial value $M_i = 0.484$ (20% less than its original mass $M = 0.605$). We can observe that initially the oscillaton expands and then bounces back while it loses mass, to finally settle down on the S-branch. The migration is manifest in the trajectory shown in figure 11, which oscillates around the stable equilibrium configurations discussed in the previous section. During the evolution, the oscillaton maintains a fixed vibration frequency. Its path of migration is labelled A in figure 8, and shows that the oscillaton will stop at a diluted one.

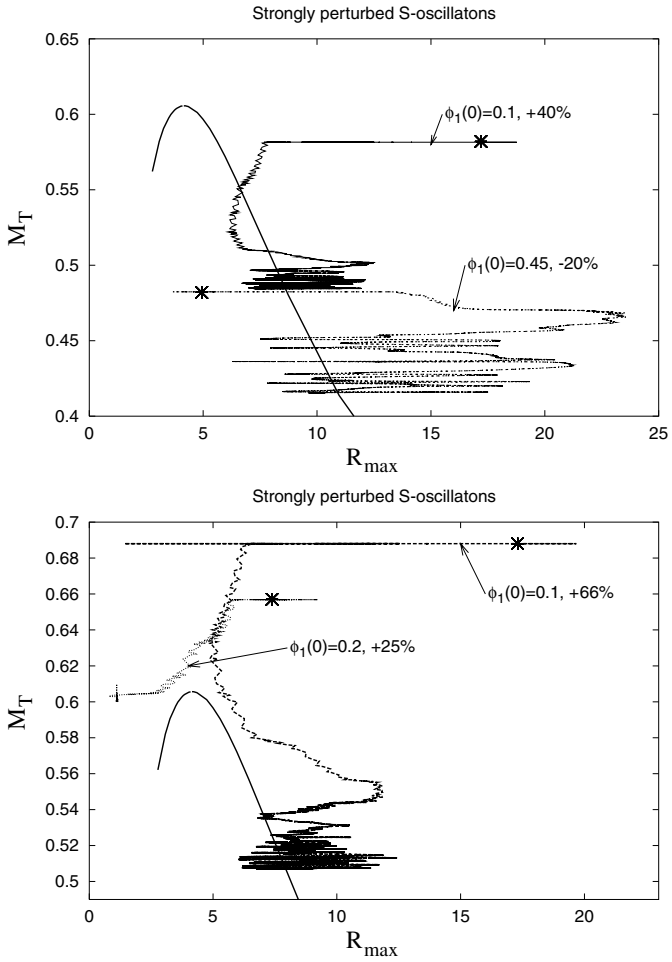

Figure 11. Evolutions of different strongly perturbed S-oscillatons, see text for details and cases labelled A–C in figure 8. The percentage figures are the perturbations made in their original masses. In general, a perturbed S-oscillaton migrates back to the S-branch if its initial mass is less than the critical value $M_c = 0.606$. The migration proceeds by the loss of mass, through the so-called gravitational cooling mechanism. This mechanism is so efficient in the case of dilute oscillatons that it can prevent the formation of a black hole even if the initial mass is larger than the critical value. However, this cooling mechanism is sometimes not enough for dense oscillatons. The asterisks denote the starting points. The runs were followed up to $t = 5000\ \mathrm{m}^{-1}$.

A second case corresponds to a $\phi_1(0) = 0.1$ oscillaton which was strongly perturbed as having an initial mass of $M_i = 0.579$ (40% over its original mass $M = 0.414$). Despite the strong perturbation, the oscillaton collapses and loses enough mass to settle down onto another S-oscillaton. By measuring the vibration frequency, we find that the migrating oscillaton follows the path labelled B in figure 8, which suggests that the oscillaton is migrating to a $\phi_1(0) = 0.15$-like profile. This can also be seen in figure 12, in which the profile of the metric coefficient g_{rr} rapidly approaches and oscillates around the final configuration.

To illustrate point (iv), a $\phi_1(0) = 0.1$ oscillaton was perturbed to have an initial mass of $M_i = 0.687$, a value larger than the critical one. However, we can observe that the oscillaton rapidly loses mass and migrates back to the S-branch. Its migration path is labelled C in

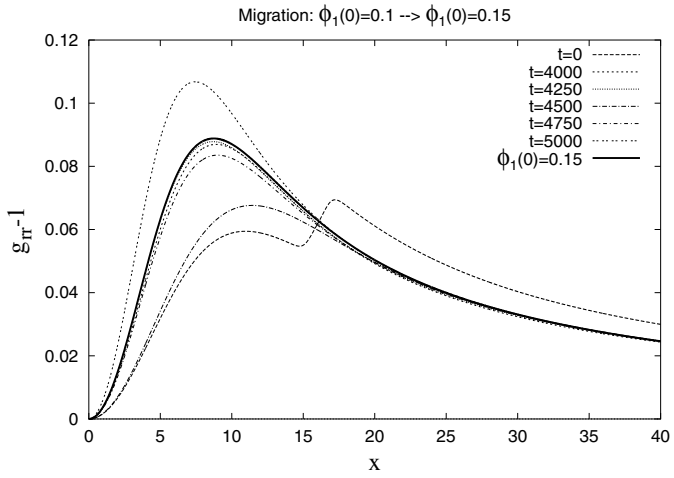

Figure 12. Evolved profiles of the metric coefficient g_{rr} for a strongly perturbed $\phi_1(0) = 0.1$ oscillaton (see also figures 10 and 11), which is migrating to a $\phi_1(0) = 0.15$ oscillaton. This is consistent with the path (labelled B) in figure 8. The times and distances are given in units of m^{-1}.

figure 8. This is a typical example of the efficiency of the gravitational cooling mechanism in sufficiently dilute oscillatons.

The opposite case is shown by a perturbed $\phi_1(0) = 0.2$ oscillaton, whose initial mass is $M_i = 0.657$. The gravitational cooling mechanism is not efficient enough in this case to prevent the formation of a black hole. We see this by noting that its trajectory stops at the value of R_{max} corresponding to the Schwarzschild radius of the hole. However, we have observed that the same oscillaton does migrate to the S-branch if the initial mass is somewhat less perturbed, while still being larger than the critical one. This is also a generic phenomenon we have observed by perturbing other S-oscillatons. This tells us that the gravitational cooling mechanism is highly efficient if the scalar field is diluted enough, as in the cases shown in the original paper of Seidel and Suen [3].

The results presented so far point out that, apart from being stable configurations, S-branch oscillatons are indeed the final states in the evolution of other perturbed S-oscillatons. These two properties (stability and final state quality) are the imprint of S-oscillatons. To end this section, we would like to stress here the important role of the quasi-normal modes to follow the migration process of oscillatons. The examples presented so far show that the vibration frequency of the system remains the same during its evolution, even while the system loses mass.

5. Evolution of oscillatons: the U-branch

We shall call U-branch oscillatons those equilibrium configurations on the right- (left-) hand side of the critical configuration in the plot of M versus $\phi_1(0)$ (M versus R_{max}) in figure 2. We also evolved these equilibrium configurations, with the same idea that the eigensolutions in section 2.1 are already slightly perturbed configurations. The main result of this section is that U-oscillatons are intrinsically unstable since, as we shall see below, they decay and migrate to the S-branch under *small* perturbations.

Shown in figure 13 are some instances of slightly perturbed U-oscillatons, and the plot of M versus R_{max} speaks by itself when compared to figure 9. The U-branch oscillatons are intrinsically unstable; they migrate to and settle down onto the S-branch, even under small

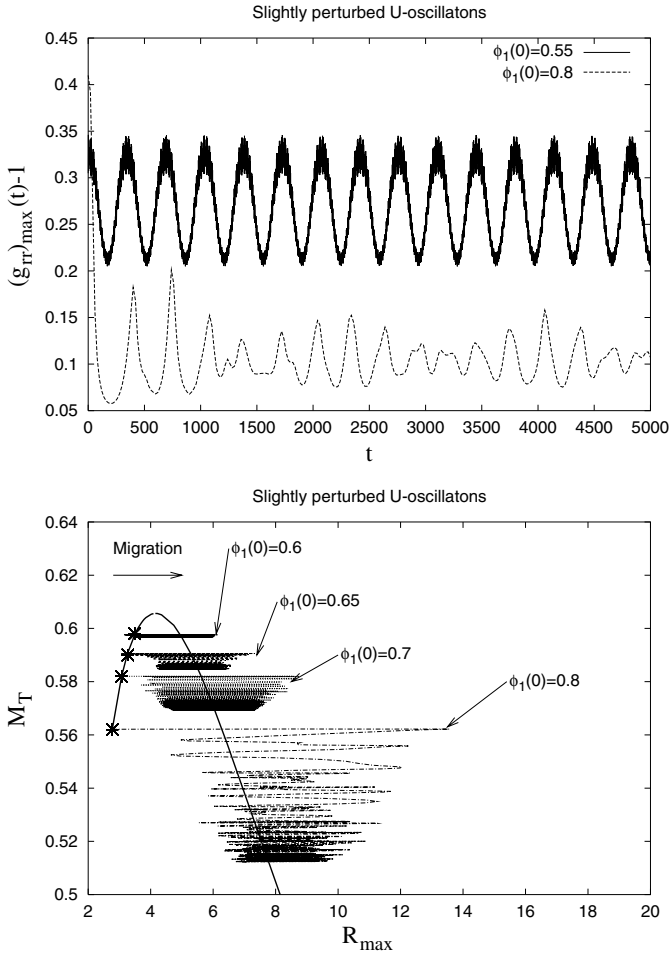

Figure 13. (Top) Evolution of the maximum value of the radial metric coefficient g_{rr} for two slightly perturbed oscillatons in the U-branch, whose corresponding central initial values are $\phi_1(0) = 0.55, 0.8$. Larger values of the latter mean more instability. (Bottom) The migration of different U-oscillatons is manifest in a graph of M versus $R_{\max}(t)$. By looking at the plot of f versus M in figure 8, we can see the point at which the different oscillatons will stop. For instance, the labels D, E correspond to the $\phi_1(0) = 0.7, 0.8$ oscillatons shown in this graph, respectively. The time is in units of m^{-1} and the asterisks denote the starting points.

perturbations. The larger the central value ($\phi_1(0) > 0.48$), the more unstable they are. Their migration to the S-branch also confirms the stability of the S-oscillatons and their important role as the final states in the evolution of migrating oscillatons.

As we have done before, the migration of oscillatons can be tracked by determining their quasi-normal frequencies. For example, the slightly perturbed $\phi_1(0) = 0.7, 0.8$ oscillatons shown in figure 13 are labelled D, E, respectively, in figure 8.

5.1. Perturbed U-oscillatons

We have also perturbed the U-branch equilibrium configurations and studied whether they migrate or collapse into black holes. The main results of this section are as follows.

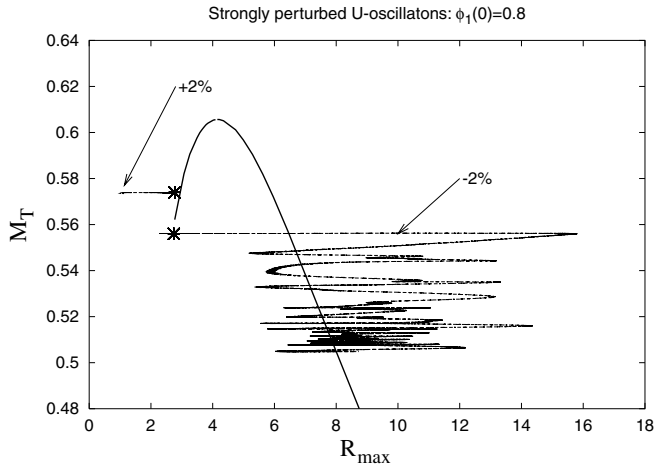

Figure 14. The paths of the evolution of a perturbed $\phi_1(0) = 0.8$ oscillaton in a plot of M versus $R_{\max}$. The collapse into the black hole is represented by the horizontal line going to the left, ending at the Schwarzschild radius of the final black hole (see also figure 15). The same oscillaton was also perturbed by decreasing its original mass, in which case it migrates and settles down into the S-branch (see text and figure 16 for details). The asterisks denote the starting points. The runs were followed up to $t = 5000\ \mathrm{m}^{-1}$.

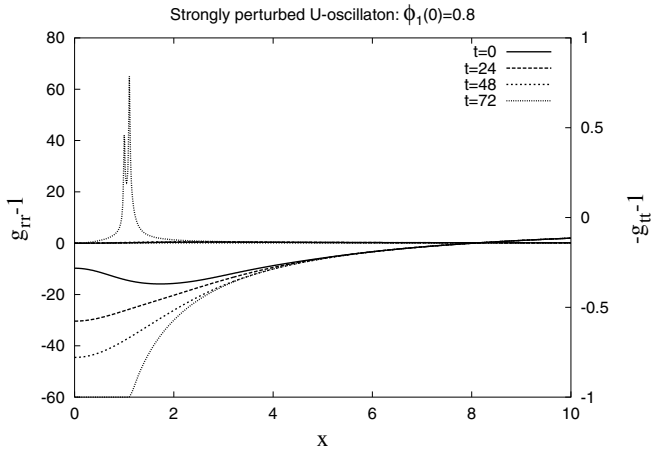

Figure 15. Plots of the metric coefficients g_{tt}, g_{rr} for a perturbed configuration with an excess mass of 2%. Even though the value of the initial mass is well below $M_c \simeq 0.606$, the oscillaton collapses into a black hole.

(i) If the initial mass is somewhat larger than the original mass of the eigenconfiguration, the oscillaton collapses into a black hole. This result is independent of the kind of perturbation made and then it can be characterized by the excess in mass only. (ii) If the mass of the original configuration is decreased by the perturbation, the oscillaton migrates to the S-branch.

The $\phi_1(0) = 0.8$ oscillaton is a typical example of a U-oscillaton and its evolution under strong perturbations is plotted in figure 14. If the initial mass of this oscillaton is perturbed so that it is 2% more massive than the original mass, the final stage of the collapse is a black hole, even though the initial mass is less than the critical value. This can also be seen in figure 15,

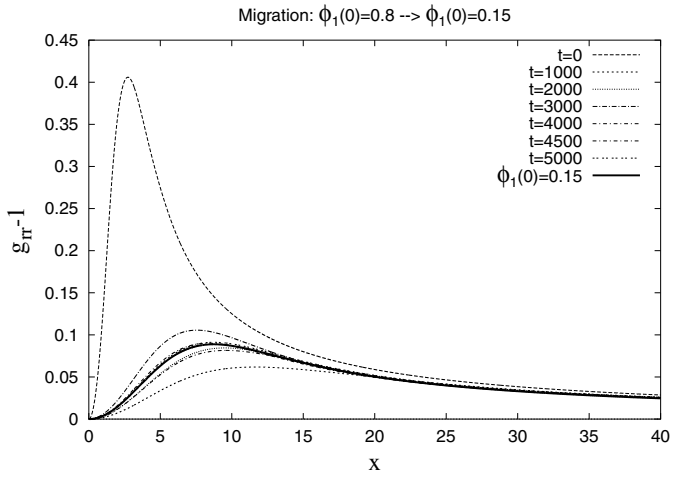

Figure 16. Evolved profile of the metric coefficient g_{rr} for a $\phi_1(0) = 0.8$ oscillaton migrating to a $\phi_1(0) = 0.15$ oscillaton. This is consistent with the graphs in figure 8 (label F) and in figure 14. The times and distances are given in units of m^{-1}.

where we see plots of the metric coefficients g_{tt} and g_{rr}. The coefficient g_{tt} shows the well-known 'collapse of the lapse' (the lapse drops to zero) characteristic of black holes, while the coefficient g_{rr} shows the 'grid stretching' effect (the radial metric grows exponentially), also typical of black hole evolutions. On the other hand, if the initial mass of the same oscillaton is 2% less than the original mass, the oscillaton rapidly migrates to the S-branch and settles down into a stable oscillaton. Its evolution path in figure 8 (label F) overlaps with that of the migrating S-oscillaton shown in figures 10 and 12 (label B in figure 8). Thus, the final state of the evolution seems to be a $\phi_1(0) = 0.15$ oscillaton, as can also be seen in figure 16. This fact reveals again the usefulness of the plot of f versus M to determine the final configuration of a migrating oscillaton.

We would like to summarize here the results presented so far. We have found that the imprint of U-branch oscillatons is that they are intrinsically unstable. That is, even small perturbations provoke their migration to other configurations, instead of small oscillations around the original ones. The latter fact again confirms the stability and final state status of S-oscillatons. Another particular characteristic of U-oscillatons is that the formation of a black hole is very likely if the original profile is perturbed by adding mass to it. This phenomenon occurs even if the perturbed initial mass is less than the critical one, so that the gravitational cooling mechanism is not efficient at all in the U-branch.

5.2. The S–U transition point

Now we take a closer look at the equilibrium configurations near the critical profile, the one that is the most massive in figure 2, which we shall call the S–U transition point.

To begin, let us recall the basic characteristics of the S, U-branches. The basic imprint of S-branch oscillatons is that they are stable and then oscillate around the initial profiles when slightly perturbed (see figure 9). On the other hand, U-branch oscillatons are intrinsically unstable and they migrate to the S-branch even when slightly perturbed, like those cases shown in figure 13.

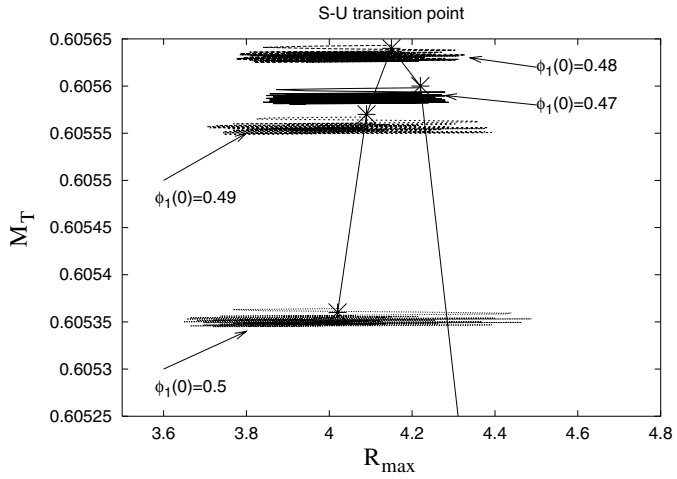

Figure 17. Evolution of slightly perturbed configurations near the S–U-transition point, which is represented by the most massive equilibrium configuration in figure 2. The oscillations of oscillatons to the right of the critical configuration are shifted to the left of the solid line, as was the general case for the S-branch (see figure 9). On the other hand, the oscillatons to the left of the critical configuration rapidly migrate to the S-branch and oscillate like stable S-oscillatons, as in figure 13. Therefore, the critical configuration truly marks the transition between the S- and U-branches.

The evolution of the profiles near the S–U transition point when slightly perturbed is shown in figure 17. We observe that the results summarized above are again confirmed, and then the critical configuration characterizes the transition between the S- and U-branches under *small* perturbations. We have also found the same results in the case of strong perturbations. If the mass of these oscillatons is decreased, they migrate to S-oscillatons. If the mass is increased even by a small amount, they collapse rapidly forming black holes.

That U-oscillatons form black holes is not surprising. The fact that S-oscillatons can also collapse to black holes near the critical point is a consequence of the inefficiency of the gravitational cooling mechanism in the case of dense S-oscillatons, as was found in section 4.1. Actually, if the mass of an S-oscillaton near the transition point is perturbed to be larger than $M > 0.606$, it will collapse into black holes; otherwise, it will migrate to more diluted configurations. That is, the value $M_c \simeq 0.606$ can be seen as the true critical value in the S–U-transition region.

Thus, we can conclude that the critical oscillaton $\left(\phi_1(0) \simeq 0.48, M_c \simeq 0.606 m_{Pl}^2/m\right)$ marks the transition from the S-branch to the U-branch.

6. Conclusions

In this paper, we have studied the properties of oscillatons by numerically evolving the Einstein–Klein–Gordon equations. According to the results, oscillatons can be classified into two well-defined groups, the S- and U-branches.

S-branch oscillatons are stable equilibrium configurations, which oscillate according to their fundamental frequency (ω). When slightly perturbed, these oscillatons vibrate with definite frequencies which we have identified as the frequencies (f) of their particular quasi-normal modes. This is supported by the fact that these vibrations are decaying amplitude oscillations around the equilibrium configurations. If these oscillatons are strongly perturbed

such that their original mass is decreased, they migrate to and settle down onto other S-branch oscillatons. This fact points out that S-oscillatons should be seen as final states to which other scalar configurations migrate.

On the other hand, we have found that S-oscillatons do not, in general, collapse into black holes if their mass is increased by the perturbation. Even though we have found that oscillatons with high central densities form black holes if their mass is larger than the critical value $M_c \simeq 0.606$, diluted oscillatons can avoid such a fate by means of the gravitational cooling mechanism. The latter can be so efficient that strongly perturbed oscillatons can migrate to stable configurations, even if their initial mass of the configuration plus that of the perturbation was much larger than the critical value.

The evolutions of the U-branch oscillatons consistently show that they are intrinsically unstable configurations. Even under small perturbations, they migrate to the S-branch. This migration also appears when they are strongly perturbed in such a way that their original mass is decreased. However, another manifestation of their unstable nature is that they rapidly collapse into black holes if their mass is increased, or simply by using the discretization error of our numerical methods.

In all cases of migrating oscillatons, we found that their evolution can be followed by measuring their vibration frequency, and this can be used to predict configuration to which the perturbed oscillatons will migrate.

In this paper, we have studied oscillatons with a quadratic scalar potential for simplicity. However, we have already initiated similar studies to include a quartic self-interaction in the potential and they will appear elsewhere.

Acknowledgments

We would like to thank Erasmo Gómez and Aurelio Espíritu for technical support, and Edward Seidel for useful discussions. TM and LAU acknowledge the kind hospitality of the AEI, where part of this work was developed. The simulations were performed in the Laboratorio de Supercómputo Astrofísico del Departamento de Física, CINVESTAV. This work was partly supported by CONACyT México, under grants 010385 (LAU), 32138-E and 34407-E. MA and DN acknowledge the DGAPA-UNAM grant IN-122002, and RB acknowledges the CIC-UMSH grant RB-4.11. This project was also partly supported by the bilateral project DFG-CONACyT 444 MEX-13/17/0-1.

References

[1] Seidel E and Suen W-M 1991 *Phys. Rev. Lett.* **66** 1659
[2] Seidel E and Suen W-M 1990 *Phys. Rev.* D **42** 384
[3] Seidel E and Suen W-M 1994 *Phys. Rev. Lett.* **72** 2516
[4] Balakrishna J, Seidel E and Suen W-M 1998 *Phys. Rev.* D **58** 104004
[5] Matos T and Guzmán F S 2001 *Class. Quantum Grav.* **18** 5055
[6] Alcubierre M, Guzmán F S, Matos T, Nuñez D, Ureña-López L A and Wiederhold P 2002 *Class. Quantum Grav.* **19** 5017 (*Preprint* astro-ph/0204307)
[7] Mielke E W and Schunck F E 2002 *Phys. Rev.* D **66** 023503
[8] Ureña-López L A 2002 *Class. Quantum Grav.* **19** 2617
[9] Ureña-López L A, Matos T and Becerril R 2002 *Class. Quantum Grav.* **19** 6259
[10] Hawley S H and Choptuik M W 2002 *Preprint* gr-qc/0208078
[11] Hawley S H and Choptuik M W 2000 *Phys. Rev.* D **62** 104024
[12] Alcubierre M, Bruegmann B, Dramlitsch T, Font J A, Papadopoulos P, Seidel E, Stergioulas N and Takahashi R 2000 *Phys. Rev.* D **62** 044034 (*Preprint* gr-qc/0003071)
[13] Teukolsky S 2000 *Phys. Rev.* D **61** 087501